Delta^4 Phantom+

Pre Treatment QA for all machines

TrueBeam, Versa HD, Radixact, Ethos
TomoTherapy, Halcyon, Unity, MRIdian

Testimonial

"The Delta^4 Phantom+ is a valuable tool for us at Herlev Hospital. We find great value in an independent measurement of the treatment plans. At Herlev Hospital we now have a complete range of Scandidos Delta^4 products covering TrueBeams, Halcyons and MRIdian."

Ulf Bjelkengren, Technical Manager, M.Sc.,
Medical Physics, Herlev and Gentofte Hospital

QA from prescription to final fraction

Delta^4 Family one software platform for all your QA needs.

With Quality Assurance from prescription to final fraction you can now increase your workflow efficiency and be confident that the treatment dose delivered to your patient is safe.

Delta^4
by ScandiDos

Innovative and Efficient QA
www.delta4family.com

Feasibility of imaging ^{90}Y microspheres at diagnostic activity levels for hepatic radioembolization treatment planning

Britt Kunnen[a)] and Martijn M. A. Dietze
Department of Radiology and Nuclear Medicine, UMC Utrecht, P.O. Box 85500, 3508 GA Utrecht, The Netherlands
Image Sciences Institute UMC, Utrecht & University Utrecht, Heidelberglaan 100, 3584 CX Utrecht, The Netherlands

Arthur J. A. T. Braat and Marnix G. E. H. Lam
Department of Radiology and Nuclear Medicine, UMC Utrecht, P.O. Box 85500, 3508 GA Utrecht, The Netherlands

Max A. Viergever
Image Sciences Institute UMC, Utrecht & University Utrecht, Heidelberglaan 100, 3584 CX Utrecht, The Netherlands

Hugo W. A. M. de Jong
Department of Radiology and Nuclear Medicine, UMC Utrecht, P.O. Box 85500, 3508 GA Utrecht, The Netherlands

(Received 10 July 2019; revised 28 November 2019; accepted for publication 11 December 2019; published 20 January 2020)

Purpose: Prior to ^{90}Y hepatic radioembolization, a dosage of ^{99m}Tc-macroaggregated albumin (^{99m}Tc-MAA) is administered to simulate the distribution of the ^{90}Y-loaded microspheres. This pretreatment procedure enables lung shunt estimation, detection of potential extrahepatic depositions, and estimation of the intrahepatic dose distribution. However, the predictive accuracy of the MAA particle distribution is often limited. Ideally, ^{90}Y microspheres would also be used for the pretreatment procedure. Based on previous research, the pretreatment activity should be limited to the estimated safety threshold of 100 MBq, making imaging challenging. The purpose of this study was to evaluate the quality of intra- and extrahepatic imaging of ^{90}Y-based pretreatment positron emission tomography/computed tomography (PET/CT) and quantitative single photon emission computed tomography (SPECT)/CT scans, by means of phantom experiments and a patient study.
Methods: An anthropomorphic phantom with three extrahepatic depositions was filled with ^{90}Y chloride to simulate a lung shunt fraction (LSF) of 5.3% and a tumor to nontumor ratio (T/N) of 7.9. PET /CT (Siemens Biograph mCT) and Bremsstrahlung SPECT/CT (Siemens Symbia T16) images were acquired at activities ranging from 1999 MBq down to 24 MBq, representing post- and pretreatment activities. PET/CT images were reconstructed with the clinical protocol and SPECT/CT images were reconstructed with a quantitative Monte Carlo-based reconstruction protocol. Estimated LSF, T/N, contrast to noise ratio of all extrahepatic depositions, and liver parenchymal and tumor dose were compared with the phantom ground truth. A clinically reconstructed SPECT/CT of 150 MBq ^{99m}Tc represented the current clinical standard. In addition, a ^{90}Y pretreatment scan was simulated for a patient by acquiring posttreatment PET/CT and SPECT/CT data with shortened acquisition times.
Results: At an activity of 100 MBq ^{90}Y, PET/CT overestimated LSF [+10 percentage point (pp)], underestimated liver parenchymal dose (−3 Gy/GBq), and could not detect the extrahepatic depositions. SPECT/CT more accurately estimated LSF (−0.7 pp), parenchymal dose (−0.3 Gy/GBq) and could detect all three extrahepatic depositions. ^{99m}Tc SPECT/CT showed similar accuracy as ^{90}Y SPECT/CT (LSF: +0.2 pp, parenchymal dose: +0.4 Gy/GBq, all extrahepatic depositions visible), although the noise level in the liver compartment was considerably lower for ^{99m}Tc SPECT/CT compared to ^{90}Y SPECT/CT. The patient's SPECT/CT simulating a pretreatment ^{90}Y procedure accurately represented the posttreatment ^{90}Y microsphere distribution.
Conclusions: Quantitative SPECT/CT of 100 MBq ^{90}Y could accurately estimate LSF, T/N, parenchymal and tumor dose, and visualize extrahepatic depositions. © *2019 The Authors. Medical Physics published by Wiley Periodicals, Inc. on behalf of American Association of Physicists in Medicine* [https://doi.org/10.1002/mp.13974]

Key words: dosimetry, PET/CT, radioembolization, SPECT/CT, yttrium-90

1. INTRODUCTION

Prior to ^{90}Y radioembolization treatment of liver tumors, a dosage of ^{99m}Tc-macroaggregated albumin (^{99m}Tc-MAA) is administered to simulate the distribution of the ^{90}Y-loaded microspheres. This pretreatment safety procedure is mainly performed to estimate the lung shunt fraction (LSF) and to detect potential extrahepatic depositions.[1] In addition, a

single photon emission computed tomography/computed tomography (SPECT/CT) scan of ^{99m}Tc-MAA may be used for intrahepatic dosimetry.[2]

The prescribed activity of ^{90}Y microspheres can be calculated based on the body surface area (BSA)-method for resin microspheres or the mono-compartment model for glass microspheres.[3,4] Both methods assume a uniform dose distribution within the (targeted) liver volume, and thereby neglect individual patient's dose distribution. Another model to calculate prescribed activity is the partition model, which takes the average tumor to nontumor ratio into account.[5] However, this method may still be an oversimplification in the case of multiple tumors with varying uptake.[2] As an alternative to the tumor to nontumor ratio, the tumor dose may be maximized based on the maximal parenchymal dose.[6]

All image-based dosimetry methods rely on the accuracy of the pretreatment procedure, which is often limited in case of ^{99m}Tc-MAA. Observed differences in ^{99m}Tc-MAA and ^{90}Y-microsphere distributions could be caused by their differences in shape and size and by free circulating pertechnetate.[7–9] A better representation of the microsphere distribution may be achieved by using identical particles for pretreatment and treatment, as is feasible in ^{166}Ho microsphere radioembolization.[10,11]

A similar objective may be pursued for ^{90}Y-loaded microspheres. However, the total energy absorbed per Bq is higher for ^{90}Y than for ^{166}Ho, which limits the pretreatment activity to the estimated safety threshold of 100 MBq.[11–13] In addition, SPECT of ^{90}Y is based on Bremsstrahlung imaging, which prevents the use of a photopeak energy window and energy window based scatter correction. Quantitative SPECT can be accomplished by applying Monte Carlo based reconstruction.[14] Alternatively, ^{90}Y may be imaged using positron emission tomography (PET). However, the small positron branching ratio of ^{90}Y in combination with the required low activity for pretreatment makes PET challenging.

In an earlier study, we demonstrated the feasibility of accurately estimating the LSF of a low activity ^{90}Y-based pretreatment procedure when imaged with SPECT/CT and reconstructed with a Monte Carlo-based reconstruction model to include scatter correction.[13] In the present study it was investigated whether low activity ^{90}Y SPECT/CT and PET/CT allowed detection of extrahepatic depositions and intrahepatic dosimetry, using an anthropomorphic phantom and short acquisition scans of a clinical patient to simulate a ^{90}Y pretreatment scan.

2. MATERIALS AND METHODS

2.A. Phantom

We used an anthropomorphic thorax phantom (model ECT/TOR/P, IEL, Chilcompton, UK) with a liver compartment, lung compartments (filled with styrofoam beads), and a spine insert. Two tumor compartments were added to the liver (one solid and one necrotic tumor) and three extrahepatic depositions were added to the background volume. The extrahepatic depositions were located posterior to the liver and below the left lung (small extrahepatic deposition), posterior to the liver and below the right lung (medium sized extrahepatic deposition) and above the liver and in between the lungs (large extrahepatic deposition; Fig. 1).

The phantom was filled with 2.0 GBq ^{90}Y chloride in 0.5 M of HCl to prevent adhesion to the plastic phantom walls.[15] The initial activity, size, and shape of all compartments are listed in Table I. The phantom had a LSF of 5.3% and a tumor to nontumor ratio (T/N) of 7.9. Based on the results of a previous study by Prince et al., the activity concentration of the extrahepatic depositions was chosen to be 1.3% of the total activity in the phantom divided by 6.8 mL.[11]

To represent the current clinical pretreatment procedure using ^{99m}Tc-MAA, the phantom was filled in a similar manner as described above with ^{99m}Tc, with a total phantom activity of 153 MBq, an LSF of 5.2%, and a T/N of 7.6.

2.B. Image acquisition

Thirteen PET/CT and SPECT/CT scans were acquired of the anthropomorphic phantom as the ^{90}Y activity decayed from 1999 MBq down to 24 MBq. The total activity of the phantom at the time of imaging is listed in Table II. For all scans, a CT scan was made for attenuation correction and to support delineation.

All ^{90}Y PET/CT images were acquired on a Siemens Biograph mCT time of flight (TOF) scanner. Two bed positions were scanned to fit the entire phantom in the field of view. Acquisition time was 15 min per bed position, resulting in a total acquisition time of 30 min. Consecutive bed positions overlapped approximately 43%.

All ^{90}Y SPECT/CT images were acquired on a dual-head Siemens Symbia T16 scanner. Photons were acquired in a 50–250 keV energy window with the high-energy collimators mounted. Projections were acquired for 30 s per angle, using

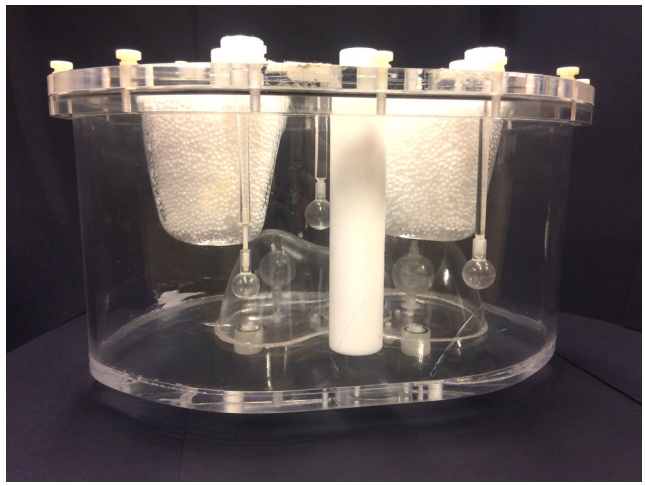

FIG. 1. Anthropomorphic phantom including liver, lung, tumor, and extrahepatic deposition compartments. [Color figure can be viewed at wileyonlinelibrary.com]

TABLE I. Initial activity, size, and shape of the compartments within the anthropomorphic phantom.

Compartment	Initial activity (MBq)	Size (mL)	Shape
Liver	1477	$1.2 \cdot 10^3$	Liver
Lungs	102	$2.1 \cdot 10^3$	Left and right lung
Solid intrahepatic tumor	158	15.9	Sphere
Necrotic intrahepatic tumor	188 (outer rim), 0 (core)	18.9 (outer rim), 5.6 (core)	Sphere inside a sphere
Small extrahepatic deposition	7	2.0	Sphere
Medium extrahepatic deposition	15	4.2	Sphere
Large extrahepatic deposition	30	8.2	Sphere

120 angles over 360°, resulting in a total acquisition time of 30 min.

The ^{99m}Tc SPECT/CT image was acquired on a dual-head Siemens Symbia T16 scanner. Photons were acquired in a 129–150 keV photopeak window and a 108–129 keV lower scatter window with the low-energy high-resolution collimators mounted. Projections were acquired for 20 s per angle, using 120 angles over 360 degrees, resulting in a total acquisition time of 20 min.

For ^{90}Y SPECT a single background measurement was performed without the phantom present using the settings described above. For ^{90}Y PET, a single long background measurement (total scan time of 24 h) was performed with the phantom without activity in the scanner. These background measurements were used to perform background corrections.

2.C. Image reconstruction

^{90}Y PET projections were reconstructed with an Ordinary Poisson Ordered Subset Expectation Maximization (OP-OSEM) reconstruction algorithm, including resolution recovery (TrueX), TOF information, random, attenuation, scatter, dead time, and decay correction. The reconstruction used four iterations with 21 subsets, and a 5 mm full width at half maximum (FWHM) Gaussian postreconstruction filter was applied. The reconstructed voxel size was $4.1 \times 4.1 \times 3$ mm^3. The background measurement was reconstructed using the same settings. Background correction was performed by subtraction (for mean or summed values) or quadratic addition (for standard deviations) of the reconstructed activity in the volumes of interest (VOIs) of the background reconstruction, from the reconstructed activity in the VOIs of the ^{90}Y reconstruction.

^{90}Y SPECT projections were reconstructed with a Monte Carlo (MC) based OSEM reconstruction algorithm, including attenuation correction, resolution recovery, and MC-based scatter correction. The background correction was performed by adding the average measured background count to the forward projection. Since MC-based reconstructions take longer to converge, the reconstruction used 60 iterations with eight subsets, and an 8 mm FWHM Gaussian postreconstruction filter was applied.[14] The reconstructed voxel size was $4.8 \times 4.8 \times 4.8$ mm^3.

^{99m}Tc SPECT projections were reconstructed using an OSEM reconstruction algorithm with flash3D, dual energy window scatter correction, and attenuation correction. The reconstruction used six iterations with eight subsets, and a 5 mm FWHM Gaussian postreconstruction filter was applied. The reconstructed voxel size was $2.4 \times 2.4 \times 2.4$ mm^3.

2.D. Analysis

The liver, lungs, tumors, and extrahepatic depositions were semi-automatically delineated on one CT scan using 3D Slicer.[16] The reference CT was rigidly registered to all other CT scans, and all VOIs were transformed accordingly, to ensure that the same volume was analyzed for each scan. Registrations and transformations were performed using Elastix and were visually inspected.[17] The liver, lungs, and extrahepatic deposition VOIs were dilated by the spatial resolution of each system (14 mm for ^{90}Y SPECT and 6 mm for ^{90}Y PET and ^{99m}Tc SPECT) to partially compensate for the partial volume effect. For ^{90}Y SPECT the dilation resulted in overlapping lung and liver VOIs, and the liver VOI was chosen to have priority over the lung VOI (as is custom in clinical practice).

2.D.1. Mono-compartment model

The mono-compartment model uses the LSF to calculate the prescribed activity for radioembolization. The LSF was calculated as:

$$\mathrm{LSF} = \frac{C_{\mathrm{lung}}}{C_{\mathrm{lung}} + C_{\mathrm{liver}}} \cdot 100\% \quad (1)$$

TABLE II. Total activity of anthropomorphic phantom at time of imaging.

Scan number	1	2	3	4	5	6	7	8	9	10	11	12	13
Total activity PET (MBq)	1966	1178	701	438	248	149	114	95	73	53	40	31	24
Total activity SPECT (MBq)	1999	1192	727	441	251	148	116	96	74	52	41	31	24

PET, positron emission tomography; SPECT, single photon emission computed tomography.

where C_{lung} is the total number of counts in the dilated lung VOI and C_{liver} is the total number of counts in the dilated liver VOI.

In addition, potential extrahepatic depositions need to be detected in a pretreatment scan. As a measure for detectability, the contrast to noise ratio (CNR) for each extrahepatic deposition was calculated as:

$$\mathrm{CNR} = \frac{\overline{extrahepatic\_deposition} - \overline{background}}{S_{\mathrm{background}}} \tag{2}$$

where $\overline{extrahepatic\_depostion}$ is the mean pixel value of the nondilated extrahepatic deposition VOI, $\overline{background}$ is the mean pixel value of the background VOI (defined as the entire phantom minus the dilated VOIs of the liver, lungs and extrahepatic depositions), and $S_{background}$ is the standard deviation of the background VOI.

The low count rate, and the ensuing high noise level, may induce false positive detection of extrahepatic depositions. To identify the presence of such false positives, spherical VOIs with the same size as the extrahepatic depositions were centered on all voxels within the phantom background VOI, and the associated CNR of these background spheres was calculated using Eq. (2), where the background is defined as the background VOI minus the background sphere. An extrahepatic deposition was considered to be detectable when its CNR was twice that of the largest CNR of the background spheres.

2.D.2. Multi compartment model

Another way to calculate the prescribed activity for radioembolization is by using the partition model, which in addition to the LSF, uses the T/N. To calculate the T/N, a parenchymal VOI was created by subtracting the tumor VOIs from the liver VOI. T/N was calculated as:

$$\mathrm{T/N} = \frac{\overline{tumor}}{\overline{parenchyma}} \tag{3}$$

where $\overline{tumor}$ is the mean pixel value of the nondilated tumor VOI and $\overline{parenchyma}$ is the mean pixel value of the nondilated parenchymal VOI.

The prescribed activity for radioembolization can also be based on a threshold for parenchymal dose and/or tumor dose. The predicted dose per GBq injected ^{90}Y was calculated as:

$$D_{\mathrm{target}} = \frac{\frac{C_{\mathrm{target}}}{C_{\mathrm{total}}} \cdot 50}{m_{\mathrm{target}}} \tag{4}$$

where C_{target} is the total number of counts in the nondilated target VOI. The target is either the parenchyma, solid tumor or necrotic tumor. Fifty is the absorbed energy in joules from the decay of 1 GBq of ^{90}Y, and m_{target} is the mass of the target VOI in kg (determined using the target VOI and a conversion factor of 1.03 g/mL).[12] C_{total} is the total number of reconstructed counts and was defined as:

$$C_{\mathrm{total}} = C_{\mathrm{liver}} + C_{\mathrm{lung}} + C_{\mathrm{extrahepatic\_depositions}} \tag{5}$$

This definition of C_{total} is based on the assumption that all injected activity ends up in either the liver or the lungs, and that for this particular phantom there is also activity located in the extrahepatic depositions.

The SPECT reconstructions were calibrated against an external source to yield Bq/mL by scaling the total number of reconstructed counts to the injected activity. The PET reconstructions already provide Bq/mL and thus it was possible to directly calculate the dose per GBq injected ^{90}Y as:

$$D_{\mathrm{target}}(\mathrm{PET\ only}) = \frac{\frac{A_{\mathrm{target}}}{A_{\mathrm{total}}} \cdot 50}{m_{\mathrm{target}}} \tag{6}$$

where A_{target} is the activity in the nondilated target VOI in GBq and A_{total} is the known total activity in the phantom in GBq.

2.D.3. Voxel-based dosimetry

Two additional metrics to those that could be used for the calculation of prescribed activity were analyzed. These are the CNR of the tumors, calculated according to Eq. (2), where the background is the parenchyma VOI eroded by the spatial resolution of each system, and the background variability (BV) of the parenchyma calculated as:

$$\mathrm{BV} = \frac{S_{parenchyma}}{\overline{parenchyma}} \tag{7}$$

where $S_{parenchyma}$ is the standard deviation of the parenchyma VOI eroded by the spatial resolution of each system and $\overline{parenchyma}$ is the mean pixel value of the parenchyma VOI eroded by the spatial resolution of each system.

2.E. Patient dosimetry

To evaluate the image quality for a more inhomogeneous activity distribution, one patient who underwent radioembolization with ^{90}Y-doped glass microspheres (TheraSphere, BTG International Ltd.) gave informed consent to receive additional scans. The patient received a total of 3.87 GBq ^{90}Y (3.12 GBq at time of PET imaging and 3.09 GBq at time of SPECT imaging). At our institute, all radioembolization patients receive a posttreatment PET/CT with the image acquisition and reconstruction settings described in the previous section.

This patient received an additional PET with shortened acquisition time of 29 s per bed position (instead of 15 min per bed position) to simulate a pretreatment scan of 100 MBq ^{90}Y. In addition, this patient received a SPECT/CT with the image acquisition and reconstruction settings described in the previous section, and a SPECT with

shortened acquisition time of 1 s per view (instead of 30 s per view) to simulate a pretreatment scan of 100 MBq ^{90}Y. A SPECT background measurement was performed with an acquisition time of 29 s per view. These background projections were added to the 1 s/view projections to ensure the right noise level. Prior to performing the clinical scan, we tested whether a short scan accurately mimics a low activity scan by acquiring additional short acquisitions of the anthropomorphic phantom at 1984, 1182, and 711 MBq, and comparing the metrics described above with the anthropomorphic scan acquired at 100 MBq.

Liver VOIs were manually drawn on the low dose CTs and were split into two VOIs: a high-dose (HD) and a low-dose (LD) VOI. The HD VOI included all voxels with a concentration greater than twice the average liver activity concentration on one of the reconstructed images; the LD VOI included all remaining liver voxels. The SPECT and PET reconstructed counts were converted into units of activity by normalization of the total counts in the liver VOI to the activity administered to the patient. The absorbed dose images assumed that all emitted energy was absorbed within the voxel of origin. Mean absorbed dose and cumulative dose volume histograms were calculated for both VOIs.

3. RESULTS

3.A. Phantom study

Figure 2 shows axial and coronal views of the PET and SPECT reconstructions of the phantom. At 2.0 GBq, both ^{90}Y PET and ^{90}Y SPECT clearly visualized the solid and necrotic tumor, as well as all extrahepatic depositions. The PET reconstruction had a higher spatial resolution than the SPECT reconstruction, which led to a more apparent "cold" core of the necrotic tumor. At ~100 MBq, noise started to prevail in the PET reconstruction and the extrahepatic depositions were not visible anymore. However, for the SPECT reconstruction at ~100 MBq, all extrahepatic depositions were still visible. For ^{99m}Tc SPECT, both tumors and the extrahepatic depositions were clearly visible.

3.A.1. Mono-compartment model

Figure 3(a) shows the LSF as a function of phantom activity. PET accurately estimated the LSF [absolute difference < 1 percent point (pp)] for activities over ~1 GBq, and overestimated the LSF for activities below ~1 GBq. SPECT accurately estimated the LSF (absolute difference < 1 pp) for activities over ~50 MBq. The ^{99m}Tc SPECT estimated an LSF of 5.0% (where the true LSF was 5.2%).

Figure 3(b) shows the CNR for the extrahepatic depositions within the phantom. For both PET and SPECT the CNR of the extrahepatic depositions decreased with the phantom activity. SPECT had a higher CNR than PET, over the entire range of phantom activities. The CNR of the ^{99m}Tc SPECT was slightly higher than the CNR of ^{90}Y SPECT at ~100 MBq.

Table III shows the minimal total activity at which the extrahepatic depositions were detectable. The smaller the extrahepatic deposition, the larger the minimal total activity needed. For SPECT, all extrahepatic depositions were detectable at the activity that would theoretically be safe to use for a ^{90}Y-based pretreatment scan (100 MBq).

3.A.2. Multi compartment model

Figure 4(a) shows the estimated parenchymal dose per GBq of ^{90}Y injected. For SPECT, the estimated parenchymal dose was accurate (absolute difference < 1 Gy/GBq) over the entire range of ^{90}Y activities. For PET, scaling the reconstructed counts to the injected activity resulted in accurate parenchymal dose estimates (absolute difference < 1 Gy/GBq) for activities over ~1 GBq. Calculating the dose using the quantitative nature of PET led to underestimation of the dose for activities over ~70 MBq and to overestimation of the dose for activities under ~70 MBq. The ^{99m}Tc SPECT estimated parenchymal dose was 31.1 Gy/GBq (where the true dose was 31.3 Gy/GBq).

Figure 4(b) shows the estimated tumor dose per GBq of ^{90}Y injected. For both PET and SPECT, the tumor dose was underestimated. The estimated dose of the solid tumor was

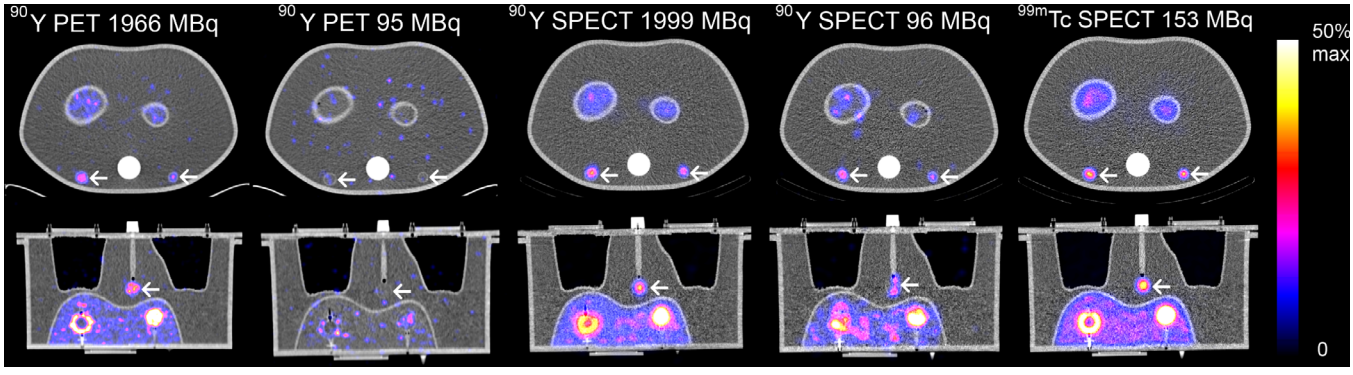

FIG. 2. Axial (top row) and coronal (bottom row) views of the phantom with x-ray images in gray scale and nuclear images in color overlay, scaled between 0 and 50% of the maximum number of counts in the reconstruction. Arrows indicate the locations of the extrahepatic depositions. [Color figure can be viewed at wileyonlinelibrary.com]

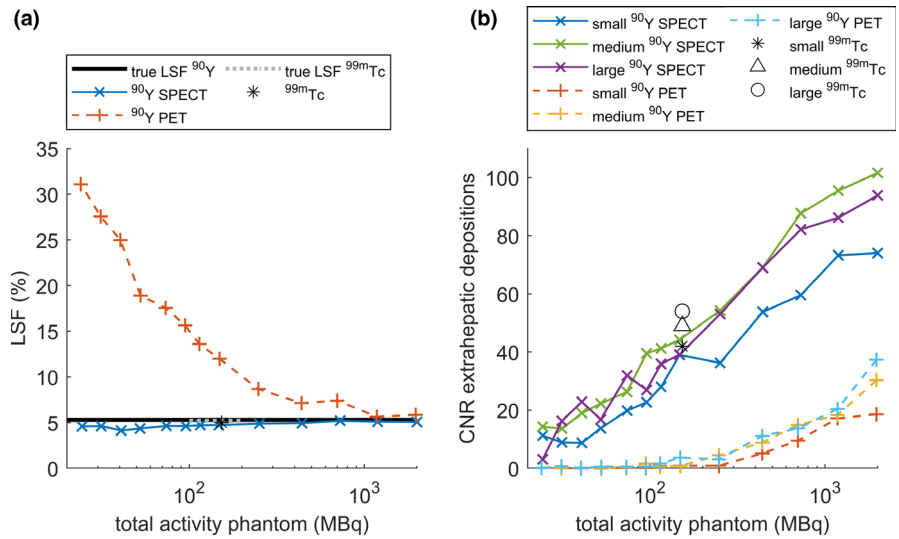

FIG. 3. (a) Lung shunt fraction as a function of total phantom activity. (b) contrast to noise ratio of the small, medium and large extrahepatic depositions as a function of total phantom activity. [Color figure can be viewed at wileyonlinelibrary.com]

larger than the estimated dose of the necrotic tumor, although differences were smaller for PET than for SPECT. For total activities over ~100 MBq, PET estimated doses of the tumors were larger than SPECT estimated doses of the tumors. For activities below ~150 MBq, PET estimated doses of the tumors started to decrease. SPECT estimated doses of the tumors were more stable over the entire range of activities. The ^{99m}Tc SPECT showed a similar estimated dose of the tumors as the ^{90}Y SPECT.

Figure 4(c) shows the T/N of the phantom. The observed trends were very similar to the trends observed for the estimated tumor dose.

3.A.3. Voxel-based dosimetry

Figure 5(a) shows the CNR of the solid and necrotic tumor. For both PET and SPECT the CNR decreased with decreasing phantom activity. SPECT had a higher CNR than PET, over the entire range of phantom activities. The solid tumor had a higher CNR than the necrotic tumor, for both modalities. The CNR of the tumors of the ^{99m}Tc SPECT was considerably higher than the CNR of the tumors of the ^{90}Y SPECT at ~100 MBq.

Figure 5(b) shows the background variability (BV) of the parenchyma. For both PET and SPECT, the BV increased with decreasing phantom activity. The BV of SPECT was lower than the BV of PET for the entire range of phantom activities. The BV of the ^{99m}Tc SPECT was considerably lower than the BV of the ^{90}Y SPECT at ~100 MBq.

3.B. Patient dosimetry

The method of adding a background measurement to the measured sinogram to achieve the right noise level for a simulated low activity scan for SPECT was tested with the anthropomorphic phantom. It showed that the simulated low activity scans acquired at a true total activity of 1984, 1182 and 711 MBq resemble a measured low activity scan of 100 MBq quite well in terms of LSF (difference <0.1 pp), parenchymal dose (difference <0.5 Gy/GBq) and tumor dose (difference <20 Gy/GBq). We therefore conclude that the simulated 100 MBq scan of the patient was a good indicator for the image quality of a ^{90}Y-based pretreatment scan.

Figure 6 shows the dose volume histograms and the axial slices of the dose maps of the SPECT scan of the patient at long and short acquisitions times. Visually, the dose maps were very similar. Quantitatively, the dose volume histograms were similar and the mean dose for the LD and HD VOIs were in close agreement (mean doses HD: 497 and 518 Gy, mean doses LD: 32.5 and 28.1 Gy, D50% HD: 405 and 407 Gy, D50% LD: 3.6 and 1.8 Gy, for long and short acquisition times respectively).

TABLE III. Total activity in the phantom (and activity concentration of the extrahepatic depositions between parentheses) at which extrahepatic depositions were detectable.

	Large deposition	Medium deposition	Small deposition
PET	>~300 MBq (0.6 MBq/mL)	>~300 MBq (0.6 MBq/mL)	>~1000 MBq (1.9 MBq/mL)
SPECT	>~30 MBq (0.06 MBq/mL)	>~45 MBq (0.08 MBq/mL)	>~90 MBq (0.2 MBq/mL)

PET, positron emission tomography; SPECT, single photon emission computed tomography.

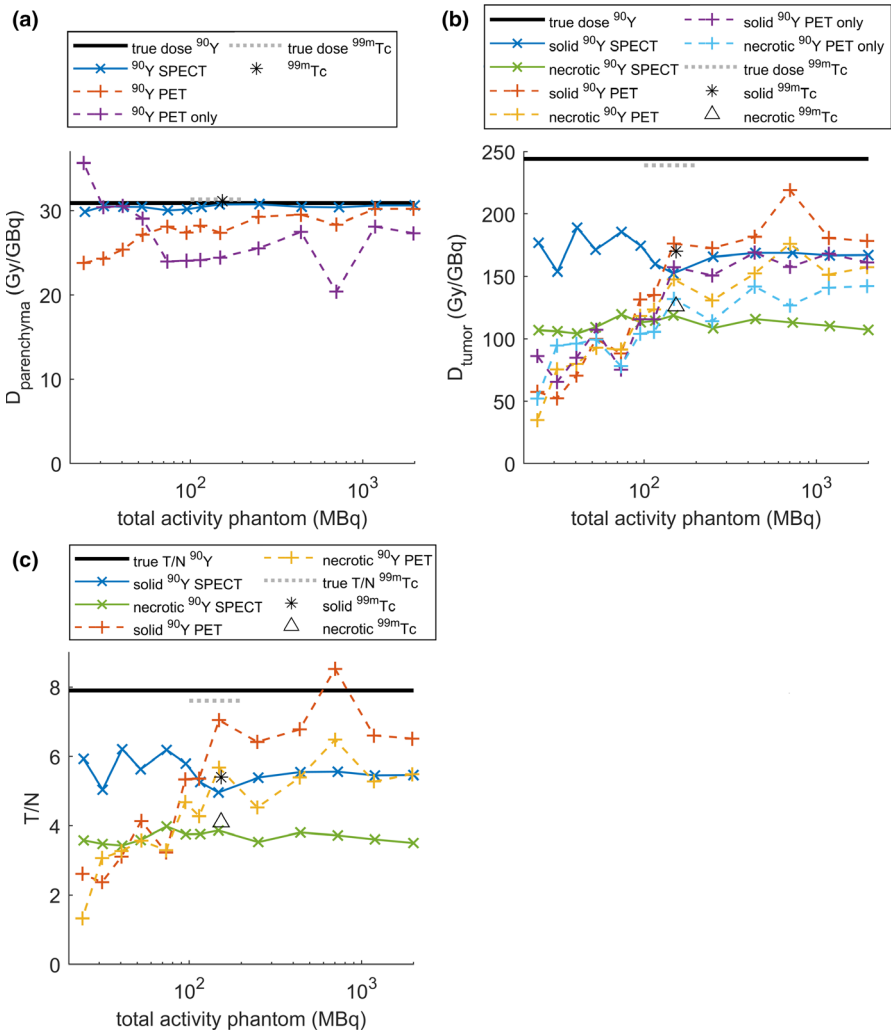

FIG. 4. Dose to the parenchymal tissue (a) and tumors (b) per GBq of ^{90}Y injected as a function of total activity in the phantom. (c) T/N as a function of total activity in the phantom. [Color figure can be viewed at wileyonlinelibrary.com]

Figure 7 shows the dose volume histograms and the axial slices of the dose maps of the PET scan of the patient at long and short acquisition times. Visually, the short acquisition reconstruction was a lot noisier than the long acquisition reconstruction. Although the mean doses for the LD and HD VOIs were relatively comparable, the dose volume histograms showed differences, implying substantial differences in dose distribution (mean doses HD: 608 and 663 Gy, mean doses LD: 16.0 and 6.2 Gy, D50% HD: 482 and 328 Gy, D50% LD: 2.0 and 0.0 Gy, for long and short acquisition times respectively).

4. DISCUSSION

This study showed that the image quality of a ^{90}Y pretreatment SPECT/CT scan (100 MBq), when reconstructed with an MC-based reconstruction model, was sufficiently accurate for LSF, T/N, parenchymal, and tumor dose estimation and that extrahepatic depositions could be detected. A simulated ^{90}Y pretreatment (100 MBq) SPECT/CT scan of a radioembolization patient showed accurate dosimetry. Furthermore, our previous results on accurate LSF estimation with ^{90}Y SPECT/CT were confirmed.[13]

The estimates of T/N and tumor dose were lower than the true T/N and tumor dose for both PET and SPECT, even at high phantom activities. This is caused by the partial volume effect. PET has a higher spatial resolution than SPECT and therefore the partial volume effect was more severe in SPECT than in PET (at 2.0 GBq, PET had a higher estimated T/N and tumor dose than SPECT). The partial volume effect also explains the higher estimated T/N and tumor dose of the solid tumor as compared with the necrotic tumor, since the solid tumor had a smaller surface-volume ratio than the necrotic tumor. The increase in underestimation of T/N and tumor dose at low phantom activities for PET is caused by the dominant noise component in these images (at 24 MBq, 61% of the true coincidences could be attributed to background activity).

To determine the detectability of extrahepatic depositions in a scan, ideally an observer study should be performed. Since this is not possible for a phantom study, we chose to compare the CNR of the extrahepatic depositions with the

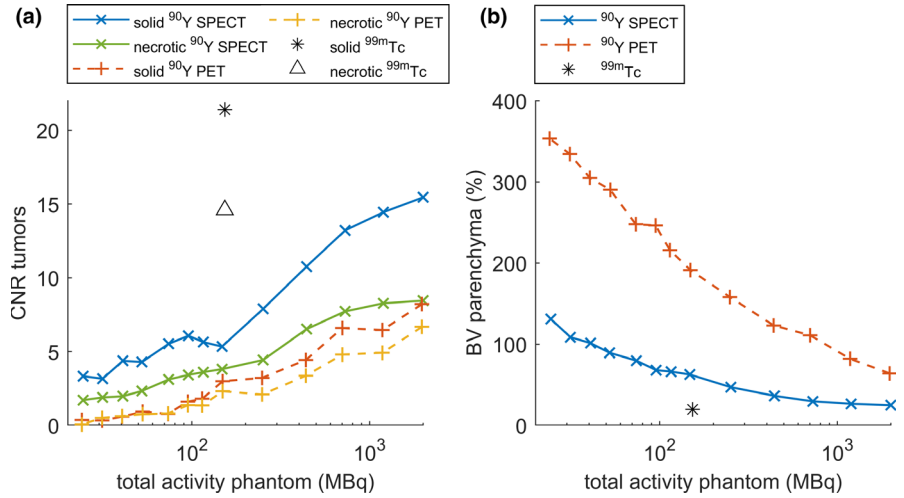

FIG. 5. (a) Contrast to noise ratio of the solid and necrotic tumor as a function of total activity in the phantom. (b) Background variability of the parenchyma as a function of total activity in the phantom. [Color figure can be viewed at wileyonlinelibrary.com]

CNR of spheres placed in the cold background of the phantom, to study false positive detection. As a threshold value for detectability we chose a factor of two for the ratio between those CNRs in order to avoid background spheres that have similar visibility as the extrahepatic depositions.

The clinical standard for the pretreatment procedure is the use of ^{99m}Tc-MAA. ^{99m}Tc, with its single photopeak, is easier to image than ^{90}Y, which has a broad Bremsstrahlung spectrum. Furthermore, ^{99m}Tc is usually imaged with a low-energy collimator instead of the high-energy collimator used for ^{90}Y, and therefore ^{99m}Tc images are expected to have a better spatial resolution. It is thus expected that a pretreatment ^{99m}Tc-MAA SPECT will have a higher image quality than a pretreatment ^{90}Y SPECT. Even though image quality of pretreatment ^{99m}Tc-MAA SPECT is superior, as followed from the CNR for the extrahepatic depositions, CNR of the tumors, and background variability of the parenchyma, the quantitative measures LSF, T/N, parenchymal, and tumor dose were comparable for both ^{99m}Tc and ^{90}Y pretreatment scans.

Current guidelines on dosage calculation from the manufacturers of microspheres are all based on a mono-compartment model and advise to determine the LSF before proceeding with radioembolization treatment.[3,4,18] This makes the LSF the most significant metric of this study for current clinical practice. A different approach to dosage calculation is to use a multi-compartment model, which would be more personalized. This requires a T/N ratio (partition model) for dosage calculation. The downside of using the T/N ratio is that there is currently no consensus on how to calculate the T/N and how to deal with multiple tumors.[2] Chiesa et al.[6] proposed to use a multi-compartment model using the parenchymal dose as input for dosage calculation. Both LSF and parenchymal dose are metrics that could be accurately estimated by ^{90}Y SPECT in this study. When moving toward voxel level estimates, a metric like the background variability (BV) becomes important. The BV favors the ^{99m}Tc SPECT, which has a considerably lower BV than ^{90}Y SPECT. However, the dose volume histograms of the

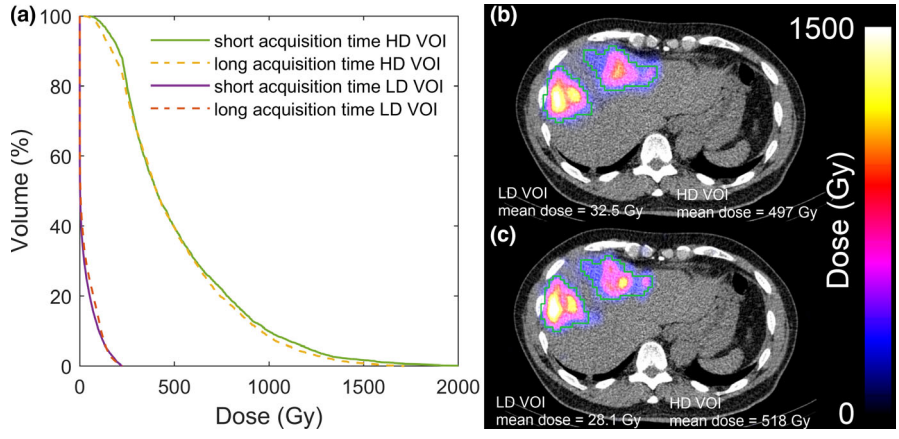

FIG. 6. Cumulative dose volume histograms of the single photon emission computed tomography/computed tomography scans with long and short acquisition times (a). Axial slice of the dose map of the long acquisition time (b) and of the short acquisition time (c). The green delineation represents the high dose volumes of interest (VOI). The low dose VOI consists of the remaining liver. [Color figure can be viewed at wileyonlinelibrary.com]

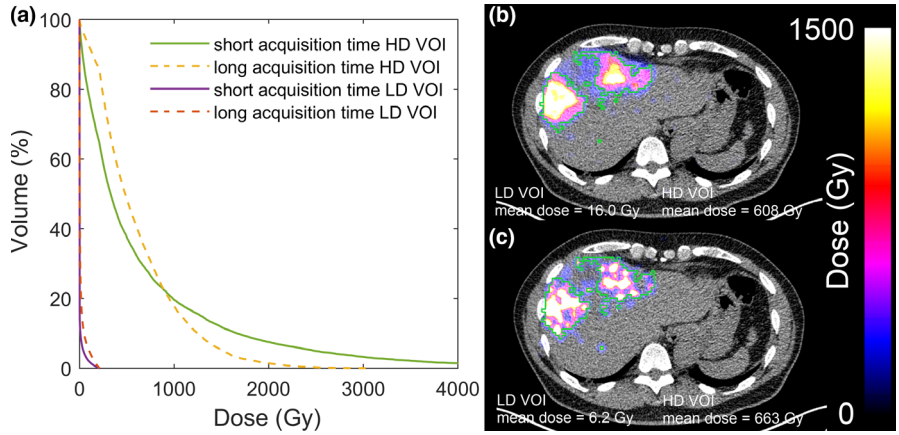

FIG. 7. Cumulative dose volume histograms of the positron emission tomography/computed tomography scan with long and short acquisition times (a). Axial slice of the dose map of the long acquisition time (b) and of the short acquisition time (c). The green delineation represents the high dose volume of interest (VOI). The low dose VOI consists of the remaining liver. [Color figure can be viewed at wileyonlinelibrary.com]

single patient show promising results, which might imply that voxel level estimates could be achievable for diagnostic activity ^{90}Y SPECT.

From a biological point of view, it is expected that using ^{90}Y microspheres instead of ^{99m}Tc-MAA for the pretreatment procedure will lead to a distribution that is more similar to the treatment procedure, since the same particle is used for the pretreatment and treatment procedures. In combination with accurate imaging, this can lead to more accurate dose planning. However, since microspheres are not metabolized,[19] the microspheres administered during a pretreatment procedure will still be present in the liver vasculature during the treatment procedure, which could change the vasculature and limit the prognostic value of the pretreatment procedure. It may be important to not only limit the activity of the pretreatment procedure to avoid unintended radiation damage, but also to limit the number of microspheres administered to avoid an embolic effect. The ideal number of microspheres that should be used for a pretreatment procedure needs further investigation.

A limitation of our study is that, owing to practical reasons, only one phantom configuration was scanned. The extrahepatic depositions all had the same activity concentration, and only three depositions were inserted in our phantom. The volumes of our extrahepatic depositions covered the lower end of the range of extrahepatic depositions described by Prince et al. (1.1–41.3 mL).[11] The same holds for the activity, where our extrahepatic depositions contained 0.35%, 0.76%, and 1.52% of the total activity, while Prince et al. found extrahepatic deposition activity ranging from 0.1% to 19.5%. Although based on this phantom experiment we cannot state that all extrahepatic depositions found by Prince et al. (on ^{99m}Tc-MAA SPECT) would be visible on a 100 MBq ^{90}Y SPECT, the majority of these extrahepatic depositions would likely be visible, because our phantom was on the lower end of both volume and activity, and we can assume that larger and/or more active extrahepatic depositions will be easier to visualize.

Due to the single phantom configuration, this study only investigated image quality of a phantom representing a radioembolization patient with a T/N of 7.9. A wide range of T/N has been reported in patients.[5,20] The results from this study cannot be directly extrapolated to distributions with other T/N, although the CNR of the tumors would most likely go down for tumors with a lower T/N.

Another limitation of the phantom is that the activity distribution within the phantom compartments was uniform, and did not represent a clinical setting. Therefore, we included a patient scan to evaluate the image quality for a more inhomogeneous activity distribution. There is no ground truth distribution for the patient scan, however, compared to the long acquisition time scan, results were comparable.

The SPECT data were reconstructed with an MC-based reconstruction algorithm, which is currently not available for clinical practice. However, the image quality of the ^{90}Y SPECT scan relies heavily on the scatter correction offered by the MC-based reconstruction model, which has also been implemented by other groups.[21,22] For availability of the MC-based reconstruction algorithm, please contact the authors.

A next step toward implementation of a ^{90}Y-based pretreatment procedure would be a patient study with several patients who receive both a pretreatment ^{99m}Tc-MAA SPECT and a pretreatment ^{90}Y SPECT for comparison. Another option is to simulate the pretreatment ^{90}Y SPECT using a short acquisition time as was done in this study.

5. CONCLUSIONS

In this phantom study, a ^{90}Y pretreatment SPECT/CT scan (100 MBq), reconstructed with a Monte Carlo-based reconstruction model, was found to have a similar quantitative accuracy as ^{99m}Tc-MAA SPECT/CT in estimating LSF, T/N, parenchymal, and tumor dose, while it can also visualize extrahepatic depositions. The image quality of a simulated ^{90}Y pretreatment scan of a patient was visually and quantitatively similar to the posttreatment scan.

ACKNOWLEDGMENTS

This project has received funding from the European Research Council (ERC) under the European Union's Horizon 2020 Research and Innovation Program (grant agreement no. 646734).

CONFLICT OF INTEREST

MGEHL is a consultant for BTG International and Terumo. AJATB has acted as a speaker for BTG International, Sirtex Medical, and Terumo. The Department of Radiology and Nuclear Medicine of the UMC Utrecht receives research support and royalties from Quirem Medical.

[a)]Author to whom correspondence should be addressed. Electronic mail: b.kunnen@umcutrecht.nl; Telephone: +31 88 7567571; Fax: +31 88 7555491.

REFERENCES

1. Braat AJAT, Smits MLJ, Braat MNGJA, et al. ^{90}Y hepatic radioembolization: an update on current practice and recent developments. *J Nucl Med*. 2015;56:1079–1087.
2. Bastiaannet R, Kappadath SC, Kunnen B, Braat AJAT, Lam MGEH, de Jong HWAM. The physics of radioembolization. *EJNMMI Phys*. 2018;5:22.
3. Sirtex Medical. *SIR-Spheres Yttrium-90 Microspheres Package Insert (CR2014)*; 2016. https://www.sirtex.com/eu/clinicians/package-insert/
4. BTG. *TheraSphereTM Yttrium-90 Glass Microspheres - Instructions for Use*; 2015.
5. Ho S, Lau WY, Leung TWT, et al. Partition model for estimating radiation doses from yttrium-90 microspheres in treating hepatic tumours. *Eur J Nucl Med*. 1996;23:947–952.
6. Chiesa C, Mira M, Maccauro M, et al. Radioembolization of hepatocarcinoma with 90Y glass microspheres: development of an individualized treatment planning strategy based on dosimetry and radiobiology. *Eur J Nucl Med Mol Imaging*. 2015;42:1718–1738.
7. Wondergem M, Smits MLJ, Elschot M, et al. 99mTc-macroaggregated albumin poorly predicts the intrahepatic distribution of 90Y resin microspheres in hepatic radioembolization. *J Nucl Med*. 2013;54:1294–1301.
8. Lambert B, Mertens J, Sturm EJ, Stienaers S, Defreyne L, D'Asseler Y. 99mTc-labelled macroaggregated albumin (MAA) scintigraphy for planning treatment with 90Y microspheres. *Eur J Nucl Med Mol Imaging*. 2010;37:2328–2333.
9. Hung JC, Redfern MG, Mahoney DW, Thorson LM, Wiseman GA. Evaluation of macroaggregated albumin particle sizes for use in pulmonary shunt patient studies. *J Am Pharm Assoc*. 2000;40:46–51.
10. Braat AJAT, Prince JF, van Rooij R, Bruijnen RCG, van den Bosch MAAJ, Lam MGEH. Safety analysis of holmium-166 microsphere scout dose imaging during radioembolisation work-up: a cohort study. *Eur Radiol*. 2018;28:920–928.
11. Prince JF, van Rooij R, Bol GH, de Jong HW, van den Bosch MA, Lam MG. Safety of a scout dose preceding hepatic radioembolization with 166Ho microspheres. *J Nucl Med*. 2015;56:817–823.
12. Gulec SA, Mesoloras G, Stabin M. Dosimetric techniques in 90Y-microsphere therapy of liver cancer: the MIRD equations for dose calculations. *J Nucl Med*. 2006;47:1209–1211.
13. Kunnen B, van der Velden S, Bastiaannet R, Lam MGEH, Viergever MA, de Jong HWAM. Radioembolization lung shunt estimation based on a 90 Y pretreatment procedure: a phantom study. *Med Phys*. 2018;45:4744–4753.
14. Elschot M, Smits MLJ, Nijsen JFW, et al. Quantitative Monte Carlo-based 90Y SPECT reconstruction. *J Nucl Med*. 2013;54:1557–1563.
15. Park M-A, Mahmood A, Zimmerman RE, Limpa-Amara N, Makrigiorgos GM, Moore SC. Adsorption of metallic radionuclides on plastic phantom walls. *Med Phys*. 2008;35:1606–1610.
16. Fedorov A, Beichel R, Kalpathy-Cramer J, et al. 3D slicer as an image computing platform for the quantitative imaging network. *Magn Reson Imaging*. 2012;30:1323–1341.
17. Klein S, Staring M, Murphy K, Viergever MA, Pluim JP. elastix: a toolbox for intensity-based medical image registration. *IEEE Trans Med Imaging*. 2010;29:196–205.
18. Quirem Medical B.V. *Instructions for Use QuiremSpheres*; 2018. http://www.quirem.com/wp-content/uploads/delightful-downloads/2019/02/LS-1101-10_04-IFU-QuiremSpheres-Multilanguage.pdf
19. Giammarile F, Bodei L, Chiesa C, et al. EANM procedure guideline for the treatment of liver cancer and liver metastases with intra-arterial radioactive compounds. *Eur J Nucl Med Mol Imaging*. 2011;38:1393–1406.
20. Goldin D, Campbell J, Emerson S, et al. Tumor-to-normal particle deposition ratio in primary versus secondary liver malignancies: impact on tumor dose and radioembolization treatment planning. *J Vasc Interv Radiol*. 2014;25:S89–S90.
21. Dewaraja YK, Chun SY, Srinivasa RN, et al. Improved quantitative 90Y bremsstrahlung SPECT/CT reconstruction with Monte Carlo scatter modeling. *Med Phys*. 2017;44:6364–6376.
22. Rong X, Du Y, Ljungberg M, Rault E, Vandenberghe S, Frey EC. Development and evaluation of an improved quantitative 90Y bremsstrahlung SPECT method. *Med Phys*. 2012;39:2346–2358.